catalysts

MDPI

Review

Advances in Nonprecious Metal Homogeneously Catalyzed Formic Acid Dehydrogenation

Manuel Iglesias * and Francisco J. Fernández-Alvarez *

Departamento de Química Inorgánica, Instituto de Síntesis Química y Catálisis Homogénea (ISQCH), Universidad de Zaragoza–CSIC, 50009 Zaragoza, Spain
* Correspondence: miglesia@unizar.es (M.I.); paco@unizar.es (F.J.F.-A.)

Abstract: Formic acid (FA) possesses a high volumetric concentration of H_2 (53 g L^{-1}). Moreover, it can be easily prepared, stored, and transported. Therefore, FA stands out as a potential liquid organic hydrogen carrier (LOHC), which allows storage and transportation of hydrogen in a safe way. The dehydrogenation to produce H_2 and CO_2 competes with its dehydration to give CO and H_2O. For this reason, research on selective catalytic FA dehydrogenation has gained attention in recent years. Several examples of highly active homogenous catalysts based on precious metals effective for the selective dehydrogenation of FA have been reported. Among them are the binuclear iridium-bipyridine catalysts described by Fujita and Himeda et al. (TOF = 228,000 h^{-1}) and the cationic species [IrClCp*(2,2′-bi-2-imidazoline)]Cl (TOF = 487,500 h^{-1}). However, examples of catalytic systems effective for the solventless dehydrogenation of FA, which is of great interest since it allows to reduce the reaction volume and avoids the use of organic solvents that could damage the fuel cell, are scarce. In this context, the development of transition metal catalysts based on cheap and easily available nonprecious metals is a subject of great interest. This work contains a summary on the state of the art of catalytic dehydrogenation of FA in homogeneous phase, together with an account of the catalytic systems based on non-precious metals so far reported.

Keywords: homogeneous catalysis; formic acid dehydrogenation; nonprecious metals; liquid hydrogen carriers

Citation: Iglesias, M.; Fernández-Alvarez, F.J. Advances in Nonprecious Metal Homogeneously Catalyzed Formic Acid Dehydrogenation. *Catalysts* **2021**, *11*, 1288. https://doi.org/10.3390/catal11111288

Academic Editor: Ioannis D. Kostas

Received: 7 October 2021
Accepted: 22 October 2021
Published: 26 October 2021

1. Introduction

Platinum group metals (PGMs) have played a critical role in the development of modern homogeneous catalysis, shaping the landscape of catalyzed industrial processes, from bulk to commodity chemicals. Despite the unquestionable success of PGM-based catalysts, research on catalysts based on Earth-abundant metals (EAM) has received great interest in recent times. This renaissance of EAM-based catalysis is mainly due to concerns over sustainability, as they seem a better option than their PGM analogues owing to their global availability, low cost, and relatively low toxicity and environmental impact [1]. Particularly, 3d transition metals allow for the preparation of inexpensive and efficient catalysts from readily available sources [2–7] and, therefore, may pave the way to the development of more sustainable processes. Moreover, 3d metals do not behave simply as mimics of their 4d and 5d counterparts; on the contrary, they present a prolific reactivity mainly due to their ability to perform one-electron redox processes and straightforward ligand reorganization. To some extent, the development of well-defined 3d metal-based catalysts has been hampered by the rather unpredictable behavior of these complexes; however, the use of appropriate ligands that tame their reactivity may offer the possibility to unravel new reactions and mechanisms.

The large scale required for the implementation of global energy transformations has prompted the scientific community to aim at the development of catalysts based on abundant metals for these types of reactions. In this context, formic acid (FA) has been

proposed as a promising hydrogen carrier because of several key properties. Among them, we can highlight its volumetric capacity and energy density (53 g H_2/L, 1.77 kW·h/L, respectively), which are markedly higher than those of compressed hydrogen (23 g H_2/L, 0.767 kW·h/L, respectively, at 35 MPa and 27 °C) [8,9]. In addition, FA presents low toxicity and its dehydrogenation often affords CO-free H_2, which is crucial for fuel cell applications [10,11]. Up to the present time, many efforts have been devoted to the development of homogeneous catalysts for formic acid dehydrogenation (FADH) based on PGM metals; however, their EAM counterparts have been less explored—although remarkable advances have been reported in recent times.

Catalysts for FADH often present participative ligands that permit metal-ligand cooperation [12]. These bifunctional catalysts have been described as containing ligands able to act as a proton shuttle that may assist with key steps of the catalytic cycle; namely, the protonation of a hydride ligand to generate H_2 or the decarboxylation of formate [13–18].

Several reviews that deal with FADH have been published [12,19–25]. Catalytic processes for the dehydrogenation of FA and the hydrogenation of CO_2 to FA have been extensively reviewed by Laurenczy and Beller in 2018, including various examples of EAM catalysts [19]. Other noteworthy reviews that deal with homogeneous catalysts for FADH based on transition metal complexes have been published [20–22]. Heterogenized molecular catalysts have been reviewed in greater detail by Deligiannakis and Louloudi [23]. The examination of heterogeneous systems is beyond the scope of this review; however, for a deeper insight on this subject the interested reader may consult recent reviews [24,25]. Due to the fast development of catalytic systems for FADH based on EAM, it seems timely to summarize the most significant advances hitherto reported on this topic.

In this review, we aim to comment on the catalytic conditions required to achieve activity with homogeneous EAM while providing an examination of the reaction mechanisms. In addition, we would like to answer important questions regarding catalyst design, such as, are bifunctional catalysts essential to promote FADH by EAM? Or do participative ligands enhance the catalytic activity of EAM-complexes?

2. Transition Metal-Based Catalysts

2.1. Cobalt Homogeneous Catalysts

The first example of a cobalt catalyst for the dehydrogenation of FA was described in 1993 by Onishi [26]. Complex $[CoH\{PPh(OEt)_2\}_4]$ catalyzes the decomposition of HCOOH into CO_2 and H_2 in THF at 30 °C under Pyrex-filtered photoirradiation with a high-pressure mercury lamp and in the absence of a base, reaching a turnover number of 3 after 6 h. The proposed reaction mechanism entails the protonation of $[CoH\{PPh(OEt)_2\}_4]$ by HCOOH to give $[CoH_2\{PPh(OEt)_2\}_4][OOCH]$ as preactivation step. Photoirradiation triggers the release of dihydrogen with concomitant formation of $[Co(OOCH)\{PPh(OEt)_2\}_4]$. The last step involves the photoirradiated decarboxylation of the formate ligand to regenerate the active species (Scheme 1).

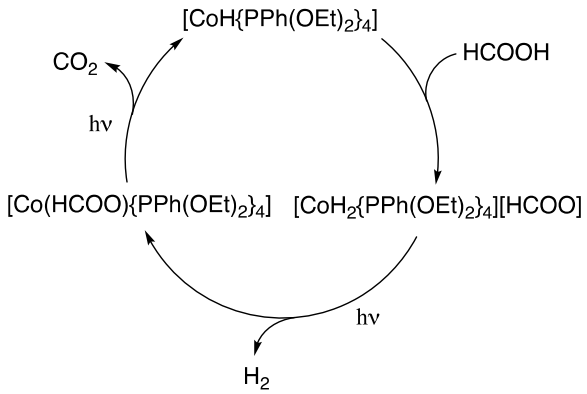

Scheme 1. Catalytic cycle proposed for the dehydrogenation of FA with $[CoH\{PPh(OEt)_2\}_4]$.

More recently, Beller and coworkers explored the activity of a series of cobalt complexes in the catalytic dehydrogenation of FA [27]. Initially, Co(II) complexes that had been previously reported to show activity in hydrogenation reactions were tested under various conditions, but no activity was detected [28]. The fact that the active species in these processes have been proposed to comprise Co(I) metal centers encouraged the authors to explore the performance of related Co(I) complexes **1**–**3** (Figure 1). These complexes were isolated and tested as catalysts in a HCOOH/DMOA mixture 10/11 (DMOA = *N*,*N*-dimethyloctylamine) at 80 °C. **1** and **2** are barely active; however, **3** showed good activities, allowing total conversion after 90 min (TON = 2260). Complex **3** also proved active in aqueous solutions employing formate as base. It is worth highlighting the extreme sensitivity of this system toward electronic/steric effects, since the exchange of the ^{i}Pr substituents of the phosphane moieties by Ph groups dramatically improves the performance of the catalyst.

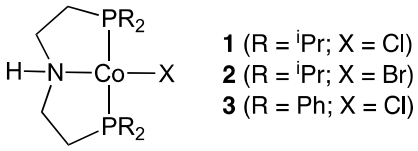

Figure 1. Depiction of complexes **1**–**3**.

The high air-sensitivity of **3** prompted the authors to evaluate the activity of the in situ generated species. **3** was formed by the reduction of the parent Co(II) complex, $[Co(Cl)_2(PNP)]$ (**4**) (PNP = bis(2-(diphenylphosphanyl)ethyl)amine), with $NaBEt_3H$ in toluene at room temperature. Subsequently, the mixture thus generated was added to the dehydrogenation system previously charged with a water solution of FA and potassium formate at 60 °C. The use of 1 equivalent of $NaBEt_3H$ resulted in lower catalytic activities than those obtained for the isolated complex, probably due to the incomplete reduction of **4**; conversely, the addition of 2 equivalents led to slightly better results than those achieved by **3**. In this regard, the authors proved that the activity of **3** with 2 equivalents of KOOCH is the same as that obtained for **4** with 3 equivalents of KOOCH, which suggests a common active species in this case.

Optimization of the reaction conditions permitted to lower the amount of KOOCH to 1 equivalent relative to FA. However, the best results were obtained at 80 °C, with a 1:4 HCOOH:KOOCH ratio and **3** as catalyst, leading to a TON value of 7166 after 70 h.

The reaction mechanism was substantiated by DFT calculations using **3** as catalyst. All the species included in the Gibbs free energy profile have triplet ground states, being the singlet states too high in energy and, therefore, discarded. The formation of the active species (**I1**) takes place via substitution of the chloro ligand in **3** by formate, which coordinates to the metal center by one of the O atoms while the other stablishes a hydrogen bond interaction with the proton of the amine. Subsequently, dissociation of the Co–O bond allows the formation of intermediate **I2**, thus allowing hydride abstraction and concomitant formation of **I3** and a molecule of CO_2. The last step brings about the formation of H_2 and the regeneration of **I1** via **TSI3-I1**, which entails hydride protonation by a molecule of FA stabilized by a hydrogen bond between the carbonyl and N–H moieties (Scheme 2). The direct protonation of the hydride by the N–H moiety or by "free" FA were discarded owing to their high energy barriers.

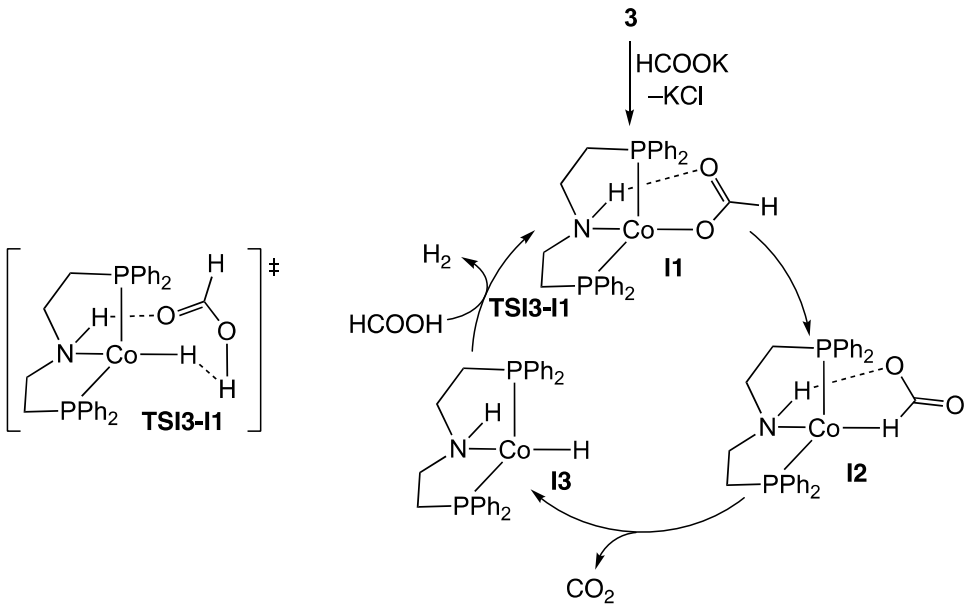

Scheme 2. Catalytic cycle proposed for the dehydrogenation of FA with **3**. The symbol "‡" denotes a transition state.

The latest example of a cobalt complex that catalyzes the dehydrogenation of FA has been reported by Cantat and coworkers [29]. This catalyst, analogously to Beller's (*vide supra*), also features an N-H moiety in the vicinity of the metal center; however, in this case no base or additives are required to achieve catalytic activity. Initially, the authors prepared Co(II) complexes **5** and **6** (Figure 2), which were reacted with five equivalents HCOOH at 150 °C, thus leading to quantitative conversion of HCOOH into CO_2 and H_2. In addition, the formation of diamagnetic species **7** (Figure 2) was detected by ^{1}H and $^{31}P\{^{1}H\}$ NMR, although its isolation was not possible by this method. The Co(I) complex **7** was prepared and successfully isolated by reaction of **5** and **6** with 3 equivalents of trimethylsilylformate at 80 °C for 16 h.

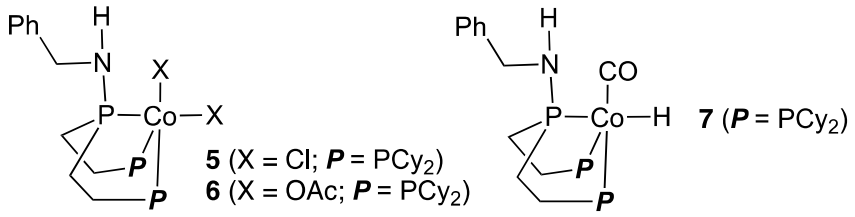

Figure 2. Depiction of complexes **5**–**7**.

The catalytic activity of complexes **5**–**7** (0.5 mol%) was evaluated at 80 °C using a solution of FA in 1,4-dioxane. Complex **5** showed no activity under these conditions, while **6** reached a TON value of 160 after 20 min, and **7** achieved full conversion in 10 min, which amounts to a TON of 200 with a TOF of 67 min^{-1}. A TON value of 458 was achieved after 4 h by means of consecutive cycles under the reaction conditions described above. It is noteworthy that **7** also showed activity in other solvents, such as toluene or water, in the absence of additives or base, although lower TON and TOF values were recorded. Computational studies on this system revealed a reaction pathway, according to which the dangling amine moiety at the PPP ligand plays a major role, allowing outer-sphere interactions with the substrate (HCOOH) by means of hydrogen bonding (Scheme 3). The initial step entails the isomerization of **7** to give intermediate **I4**, where the hydride and carbonyl ligands exchange positions relative to **7**. Subsequently, protonation of the hydride in **I4** affords a molecule of H_2 and **I5**. Subsequently, although β-hydride elimination is a possible reaction pathway, the authors found that hydride abstraction aided by a molecule

of FA, via intermediates **I6** and **I7**, was a lower energy pathway. Thus, CO_2 release renders intermediate **I4**, closing the catalytic cycle.

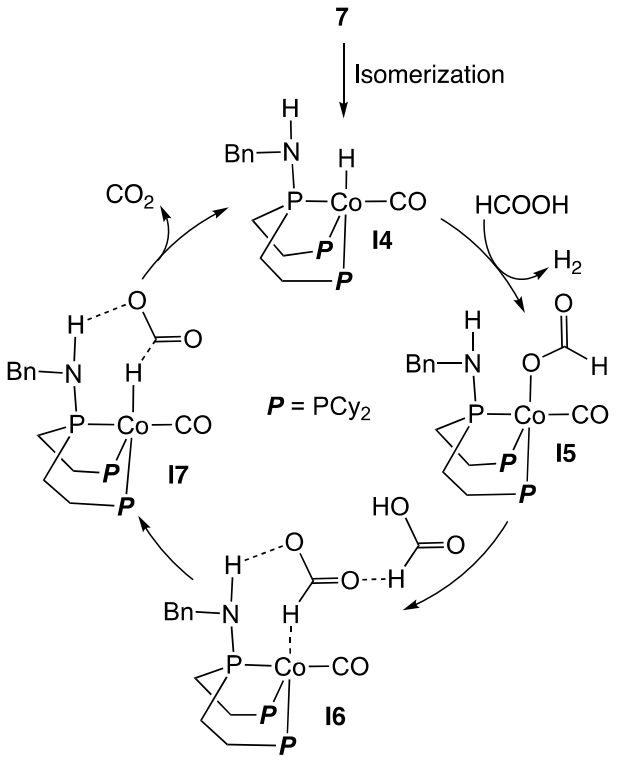

Scheme 3. Catalytic cycle proposed for the dehydrogenation of FA with **7** in the absence of base.

Remarkably, in contrast with the mechanism described above for **3** and **7**, the decarboxylation of formate without the assistance of a cooperative mechanism has been recently described for a cobalt complex [30].

2.2. Iron Homogeneous Catalysts

In 2010 Beller, Ludwig and coworkers explored the activity of a wide range of iron-carbonyl complexes in the presence of various ligands and visible-light irradiation [31]. $[Fe(CO)_5]$, $[Fe(CO)_3(COT)]$, $[Fe_2(CO)_9]$, $[Fe(CO)_3(BDA)]$ and $[Fe_3(CO)_{12}]$, (COT = cyclooctatetraene; BDA = benzylideneacetone) were tested at 40 °C under light irradiation with a 300 W xenon lamp (filtering the UV portion with a hot mirror) in a DMF solution of HCOOH and Et_3N (5:2). $[Fe_3(CO)_{12}]$ with 3 equivalents of PPh_3 and tpy (terpyridine) was found to be the best performing catalyst, closely followed by $[Fe_2(CO)_9]$ and $[Fe(CO)_3(COT)]$ with analogous ligand ratios (Fe/PPh_3/tpy 1:1:1). It is worth noting that when these ligands were used independently, a drastic drop of the catalytic activity was observed.

Experiments performed by successively turning on and off the light source showed that catalytic activity was only observed under irradiation, while dark periods revealed no gas evolution, which led the authors to conclude that the reaction was photoassisted instead of simply photoinduced.

Fine tuning of the ligand system was carried out by testing a broad variety of *P*- and *N*-ligands, obtaining the best activities with PPh_3 and 6,6″-substituted terpyridine ligands. Namely, 6,6″-(bromo)-2,2″:6′,2″-terpyridine and 6,6″-(phenyl)-2,2″:6′,2″-terpyridine delivered the highest TOF value (200 h^{-1}). Although less active, phenanthroline ligands led to higher catalyst stability.

Based on NMR, IR and DFT studies the authors proposed $[Fe(H)(CO)_3(PPh_3)]^-$ (**I8**) as the active species, which forms by irradiation of $[Fe(CO)_3(PPh_3)_2]$ in the presence of FA. The benefit of using *N*-ligands is unclear since no complex containing these ligands was identified by means of stoichiometric experiments. Nonetheless, the authors claim a

stabilizing role after phosphane dissociation, because the loss of a CO ligand was observed in the presence terpyridine, which may be a catalyst deactivation pathway. Once **I8** is generated, protonation of its hydride ligand by FA leads to formation of the dihydrogen complex **I9**. Subsequently, phosphane coordination and H_2 release renders **I10**. Finally, β-hydride elimination closes the catalytic cycle delivering a molecule of CO_2 (Scheme 4).

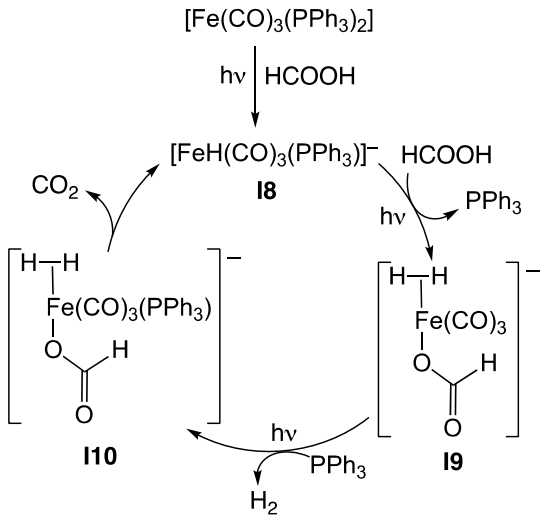

Scheme 4. Catalytic cycle proposed for the dehydrogenation of FA with $[Fe(CO)_3(PPh_3)_2]$ in situ generated from the mixture $[Fe_3(CO)_{12}]/PPh_3$/tpy.

Shortly after, Beller, Ludwig and Laurenczy developed an Fe(II) catalyst based on the tetradentate ligand $P(CH_2CH_2PPh_2)_3$ (PP_3), which was prepared in situ employing ratios Fe/ligand 1:1 and 1:2, with the latter showing better activities [32]. Remarkably, the reaction works without the need for base or additives, and using an environmentally benign solvent, namely, propylene carbonate. Moreover, high pressures of CO_2 and H_2 (up to 30 and 20 bar, respectively) showed no significant effects on the activity of the catalyst. The presence of air or the traces of water present in the solvent or FA did not affect the performance of the catalyst, but addition of chloride to the system resulted in a sharp reduction of the catalytic activity.

Several Fe-hydride complexes featuring the PP_3 ligand were tested, with $[Fe(H)(PP_3)]BF_4$ (**8**) and $[Fe(H)(H_2)(PP_3)]BF_4$ (**9**) showing better catalytic activities than the catalyst generated in situ from $[Fe(H_2O)_6][BF_4]_2/PP_3$ (1:1)—the TON_{2h} values reported for these systems were 745, 727 and 562, respectively. The activities of the systems $[Fe(H)(PP_3)]BF_4/PP_3$ (1:1) and $[Fe(H_2O)_6][BF_4]_2/PP_3$ (1:2) are very similar, with TON_{2h} values of 1227 and 1279, respectively. DFT and experimental studies on the reaction mechanism led the authors to propose two competing catalytic cycles, A and B in Scheme 5. In the case of cycle A, the first step involves the protonation of the hydride ligand in **8** to afford **I11** with concomitant release of H_2. **I11**, which is in equilibrium with an analogous species featuring a monodentate formate, undergoes β-hydride elimination to yield **I12**. Finally, CO_2 dissociation closes the cycle. Regarding cycle B, coordination of formate to **8** leads to the formation of **I13**, which renders **I14** upon protonation of the hydride and β-hydride elimination of the formate, thus generating a molecule of CO_2. Finally, H_2 dissociation restarts the cycle.

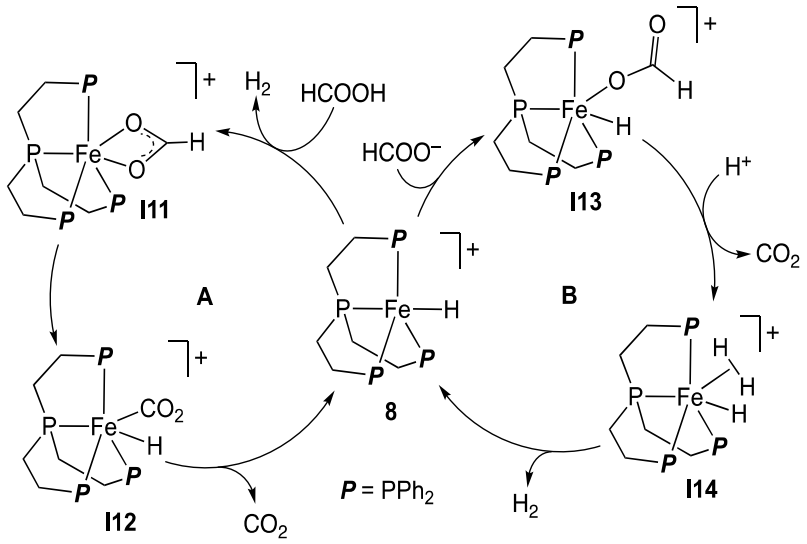

Scheme 5. Catalytic cycle proposed for the dehydrogenation of FA using complex **8** as catalyst.

Complexes **10** and **11** (Scheme 6) can catalyze the dehydrogenation of FA in the presence of a 50 mol% Et_3N at 80 °C in dioxane, allowing a TOF of 739 h^{-1} and a TON of 994 after 2.5 h for **11b** [33]. The authors showed that the use of a Lewis acid (10 mol%) instead of Et_3N gives rise to excellent catalytic activities; namely, $LiBF_4$ renders outstanding TOF and TON values (196,728 h^{-1} and 983,642, respectively)—note that in the absence of additives the system proved barely active. Mechanistic studies suggest that Et_3N is not directly involved in the catalytic cycle, since all the steps of the mechanism may take place in the absence of base. The improved activities in the presence of Et_3N and Lewis acids, such as $LiBF_4$, hint at a similar role in the reaction mechanism. The authors propose that the decarboxylation of **11**, which is the rate liming step according to kinetic experiments, takes place via hydride abstraction assisted by a Lewis acid (instead of β-hydride elimination). Rearrangement of the formate ligand yields an H-bound intermediate, which is stabilized by hydrogen bonding between the carboxylate moiety and the Lewis acid, or, in the case of Et_3N, the Brønsted acid $[Et_3NH]^+$ that forms in the presence of excess FA (Scheme 7). This lowers the activation energy of the decarboxylation step, thus improving the reaction rates.

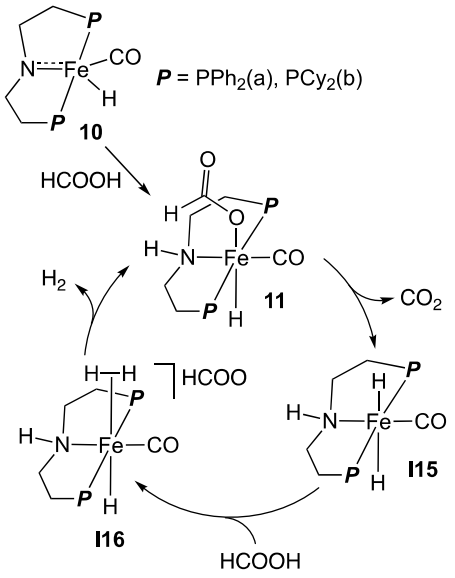

Scheme 6. Catalytic cycle proposed for the dehydrogenation of FA using **10** or **11** as catalysts.

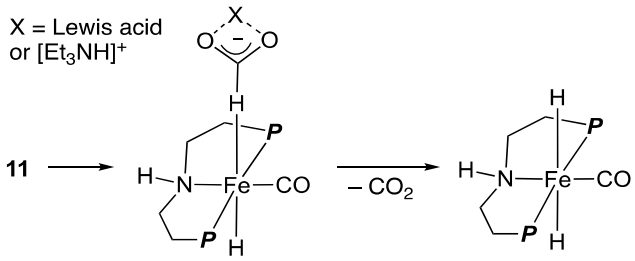

Scheme 7. Decarboxylation step assisted by a Lewis acid or $[Et_3NH]^+$.

The overall reaction mechanism entails the formation of the active species, **11**, by protonation of the amide in **10** with FA and coordination of the thus formed formate. Subsequently, decarboxylation of **11** affords dihydride **I15**, which is protonated by FA to afford **I16**. Finally, release of H_2 from **I16** regenerates the active species **11**.

The tridentate PNP ligand and the ancillary ligands about the iron center were modified to optimize the activity and stability of the catalyst [34]. However, under analogous conditions to those described above for **10** or **11** (0.1 mol% catalyst loading and 50 mol% Et_3N in dioxane at 80 °C) no significant improvement was achieved with catalysts **12–14** (Figure 3). In fact, only **13**, which is closely related to **11**, produced comparable results.

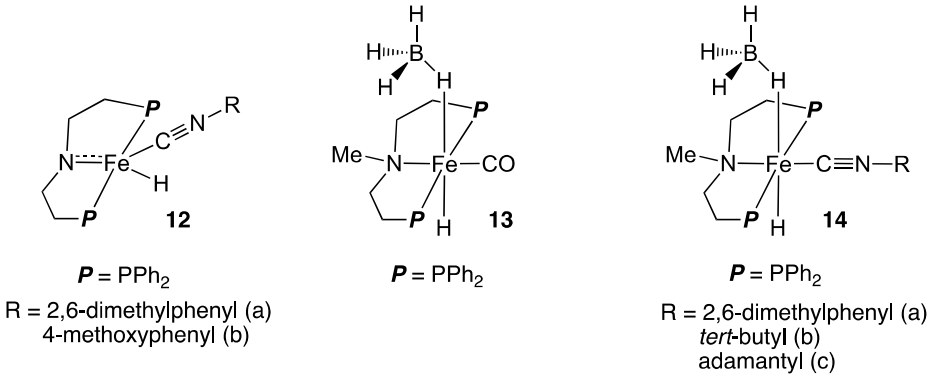

Figure 3. Depiction of catalysts **12–14**.

The group of Gonsalvi developed a series of iron complexes containing *rac*- and *meso*-1,1,4,7,10,10-hexaphenyl-1,4,7,10-tetraphosphadecane (*rac*-p4 and *meso*-P4) [35]. The preformed complex *cis*-α-$[Fe(CH_3CN)_2(rac\text{-}P4)](BF_4)_2$ (**15**) was unsuccessfully tested as catalyst in the dehydrogenation of FA. However, in situ generated catalysts from the reaction of the iron(II) salt $[Fe(H_2O)_6][BF_4]_2$ with the ligands *rac*-P4 or *meso*-P4 showed good activities in propylene carbonate at temperatures between 40 and 60 °C under isobaric conditions (1 atm). The best activities were obtained for 2:1 and 4:1 excess of *rac*-P4, reaching TON and TOF values of 6061 and 1737 h^{-1}, respectively, for the latter. The reaction of *rac*-P4 with $[Fe(H_2O)_6][BF_4]_2$ affords complex **16**, which was proposed as precatalyst.

Mechanistic studies based on NMR experiments led the authors to propose the catalytic cycle depicted in Scheme 8. The first step involves the formation of the κ^2-formate intermediate **I17**, which is in equilibrium with its **I18**. β-hydride elimination from **I19** affords the hydride intermediate **I20**. Finally, protonation of the hydride regenerates **I17** and releases H_2. It is noteworthy that under isochoric conditions the authors observe the formation of a carbonyl complex (**17**), $[FeH(CO)(rac\text{-}P4)]BF_4$, which they suggest forms from the hydride species **I20** by reaction with CO—generated by the competitive decomposition of HCOOH into CO and H_2O.

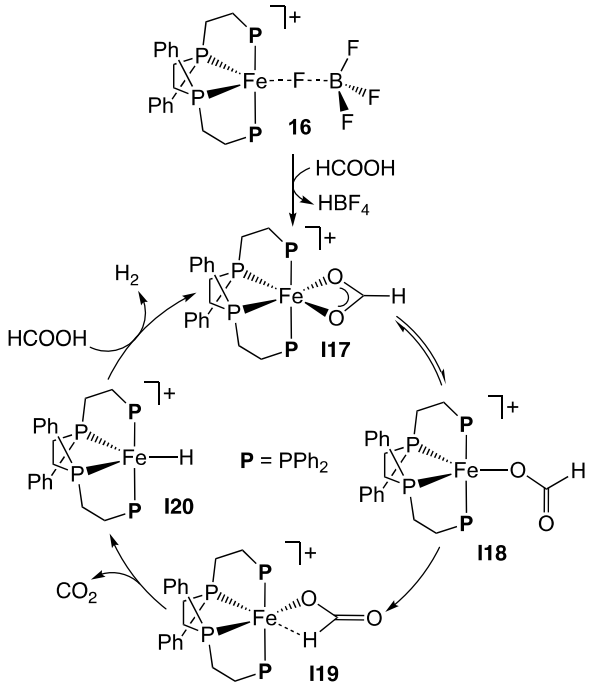

Scheme 8. Catalytic cycle proposed for the dehydrogenation of FA using **16** under isobaric conditions.

2.3. Manganese Homogeneous Catalysts

In 2016, Tondreu and Boncella reported that the Mn(I) complex [Mn(PNP)$(CO)_2$] (**18**; *P* = P^iPr_2), which is isoelectronic with the Fe(II) species **10** (Scheme 6), reacts with FA to give the 1,2-addition product [Mn(PN^HP)$(CO)_2$] (**19**) (Scheme 9). Complex **19** proved to be an active catalyst precursor for the catalytic decomposition of FA in 1,4-dioxane. The authors observed that the addition of $LiBF_4$ to the reaction mixture inhibits the catalytic activity. The low activity of this manganese-based FA-dehydrogenation catalytic system, in addition to the poor selectivity—formation of CO was observed—, makes it unsuitable for fuel cell applications [36].

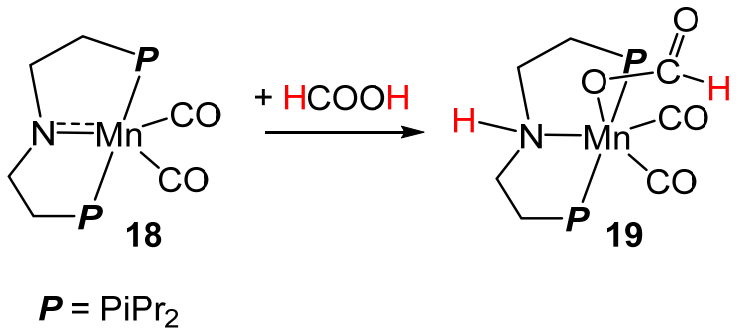

Scheme 9. Preparation of the first example of manganese-based FA dehydrogenation catalyst [Mn(PN^HP)$(CO)_2$] (**19**).

Some years later, the strategy of using the non-innocent N-H moieties in PNP ligands was applied to prepare the species [Mn($^{tBu}PN^HNOP$)$(CO)_2$]Br (**20**). The deprotonation of the cationic species **20** with $NaN(SiMe_3)_2$ yields complex [Mn(^{tBu}PNNOP)$(CO)_2$] (**21**) (Scheme 10), which is an effective catalyst precursor for the dehydrogenation of FA to H_2 and CO_2 using chlorobenzene as solvent and Et_3N as base. The highest catalytic activity for this system (TOF = 8500 h^{-1}), which is comparable to some obtained using catalytic systems based on noble metals, was achieved using one equivalent of Et_3N to FA at 80 °C [37].

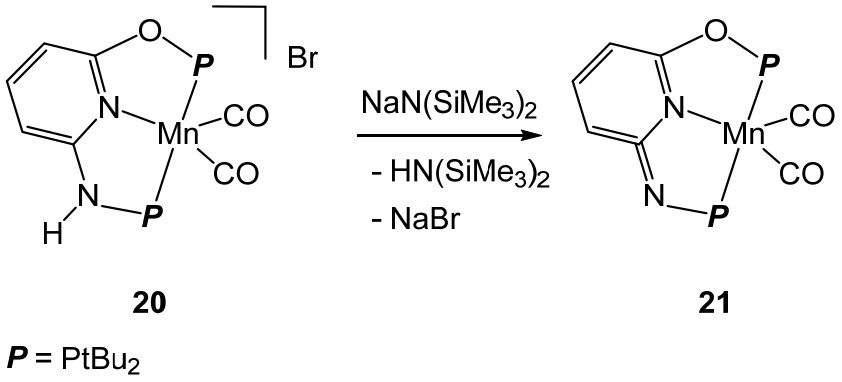

Scheme 10. Preparation of the manganese-based FA dehydrogenation catalyst [Mn(PNNOP)$(CO)_2$] (**21**).

Examples of phosphine free manganese catalysts based on bidentate Mn(I)-κ^2-*N*-*N* species, recently reported by Beller et al., proved active for the selective dehydrogenation of FA in a mixture of H_2O (9 mL) and triglyme (4 mL) in presence of KOH (1.1 equiv. to FA) at 92.5 °C. The nature of the bidentate ligand influences the catalyst activity (Figure 4) [38,39]. However, the activity of Mn(I)-κ^2-*N*-*N* species (TOF = 188–625 h^{-1}) is lower than that reported for **21**.

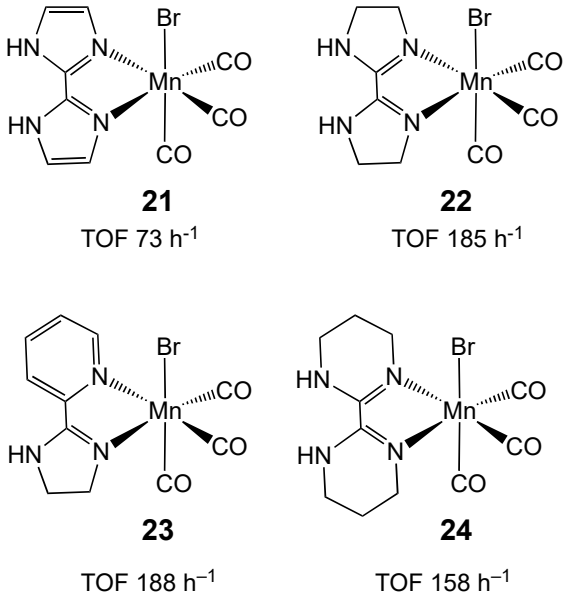

Figure 4. Examples of Mn(I)-κ^2-*N*-*N* catalyst precursors.

Britto and Jaccob have recently reported a mechanistic study at the DFT level on the **24**-catalyzed dehydrogenation of FA. They found that the formation of the Mn-formate intermediate **28** from **24** follows a dissociative mechanism (Scheme 11). The dissociation of the Br^- ion creates a vacant site, which is occupied by a molecule of solvent (H_2O). The dissociative exchange of water by the formate ion leads to intermediate **28**. The energy barrier of the activation process corresponds to **TS26-28** (23.5 kcal mol^{-1}) [40].

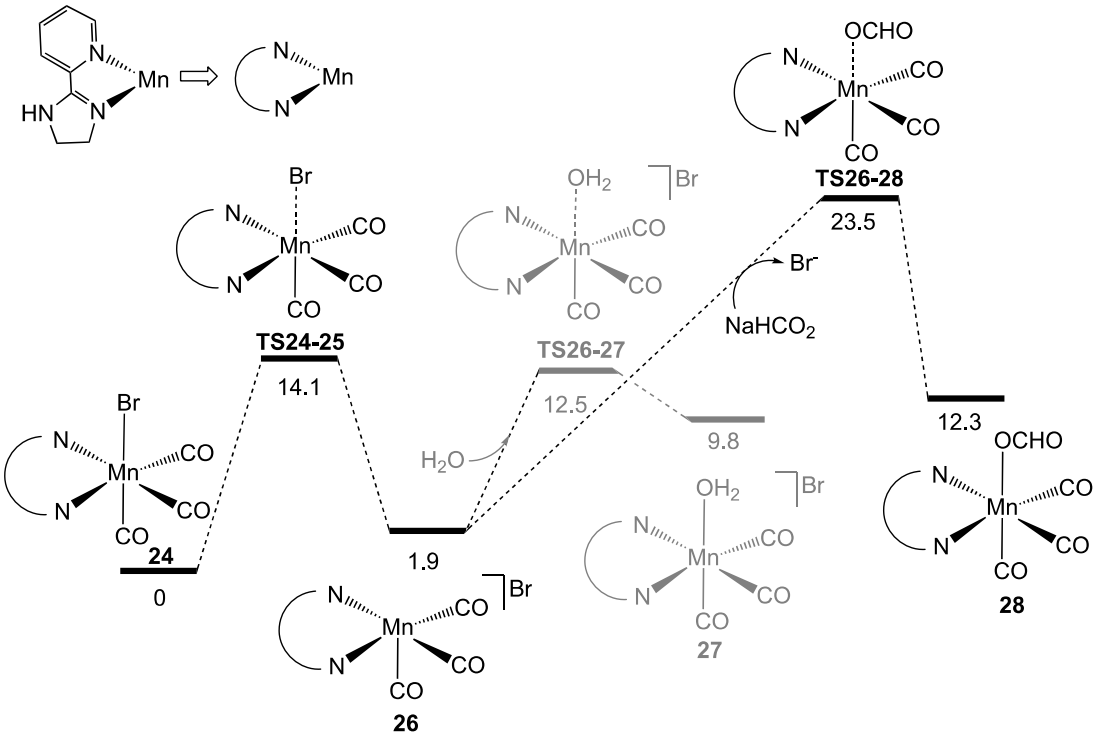

Scheme 11. Energy profile for the formation of the Mn-formate active species **28** from **24**.

Starting from the Mn-formate intermediate **28**, the β-hydrogen elimination process to give the Mn-H species **29** has been found to be the rate-determining step of the catalytic cycle (19.0 kcal mol^{-1}). The generation of H_2 occurs by protonation of the Mn-hydride with a hydronium ion instead of FA (Scheme 12). This catalytic cycle is like that proposed by Beller's group based on kinetic studies.

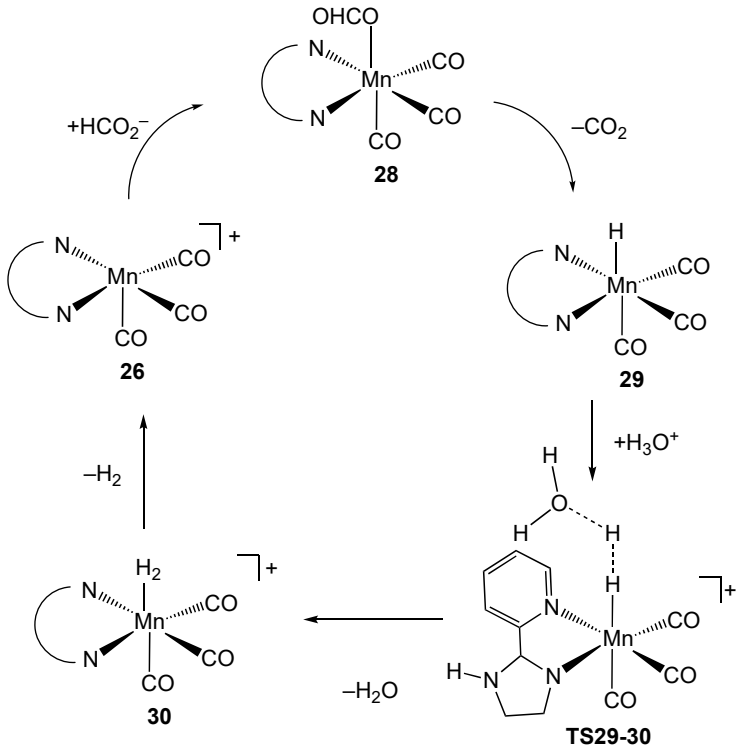

Scheme 12. Mechanism proposal for the **28**-catalyzed dehydrogenation of FA.

2.4. Nickel Homogeneous Catalysts

Although the nickel complexes hitherto tested as catalysts for FADH show little promise, a few noteworthy examples have been reported [41]. Nickel hydride complex **31** proved able to react with FA to afford H_2 and formato complex **31**. Successively, **32** releases CO_2 at 50 °C to regenerate **31** (Scheme 13). Complex **31** showed activity as an FADH catalyst with a HCOOH:dimethyl-*n*-octylamine mixture 11:10. The best results were obtained at 80 °C using propylene carbonate as solvent (TON_{3h} = 626), although the authors detected CO_2 formation from solvent decomposition.

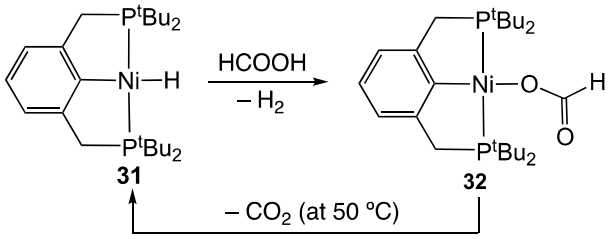

Scheme 13. Reactivity of **31** with FA in the presence of Et_3N.

Parkin and coworkers evaluated the activity of group 10 zerovalent complexes $Ni(PMe_3)_4$, $Pd(PMe_3)_4$ and $Pt(PMe_3)_4$ as catalysts in FADH. Remarkably, the nickel complex was found to be the only one to display activity, giving rise to a TON of 70 and a TOF of 1.7 h^{-1} in the absence of additives or base [42]. Based on mechanistic studies, the authors proposed the formation of a pentacoordinate Ni(II) species, $[Ni(PMe_3)_3(OOCH)(H)]$, by oxidative addition of FA with concurrent release of a PMe_3 ligand. PMe_3 dissociation and subsequent decarboxylation affords the dihydride species $[Ni(PMe_3)_2(H)_2]$, which releases H_2 triggered by PMe_3 coordination. Oxidative addition of FA regenerates $[Ni(PMe_3)_3(OOCH)(H)]$, thus restarting the catalytic cycle. Alternatively, protonation of $[Ni(PMe_3)_2(H)_2]$ by FA would also release H_2 and regenerate $[Ni(PMe_3)_3(OOCH)(H)]$ upon PMe_3 coordination. Although experimental support was found for the former pathway, the latter cannot be discarded.

2.5. Copper Homogeneous Catalysts

The first examples of Cu-catalyzed homogeneous hydrogen production from FA/amine adducts were reported in 2014. This work studies the effect of different reaction parameters on the catalytic performance. The authors found that when using Cu(II) compounds such as $Cu(AcO)_2$, $Cu(OOCH)_2$, $Cu(acac)_2$ and $Cu(NO_3)_2$,no relevant changes in the activity were observed. This demonstrated that the activation step, replacement of the ancillary ligands by formate and amine, is fast and does not determine the rate of the process. The activity of these catalytic systems improves by increasing steric hindrance and by decreasing nucleophilicity, which suggests that the role of the amine is not limited to HCOOH deprotonation. These Cu-based catalytic systems are selective to the one to one H_2:CO_2 production and only traces of CO were detected. However, the activity of all the reported examples was found to be considerably low (TOF < 1 h^{-1}) [43].

Mechanistic studies at the DFT level show that the rate-determining step of the catalytic process is the amine dissociation to generate a coordination vacancy *cis* to the formate, which is necessary for the beta β-hydrogen elimination to give a *cis*-$[CuH(NR_3)_2(\kappa^1\text{-}O\text{-}CO_2)]$ intermediate. This study confirms the experimental data, which suggest that the energetic barrier of the process depends on the nature of the amine. Thus, the use of Et_3N is preferred to NBu_3 by 1.6 kcal mol^{-1} (Scheme 14).

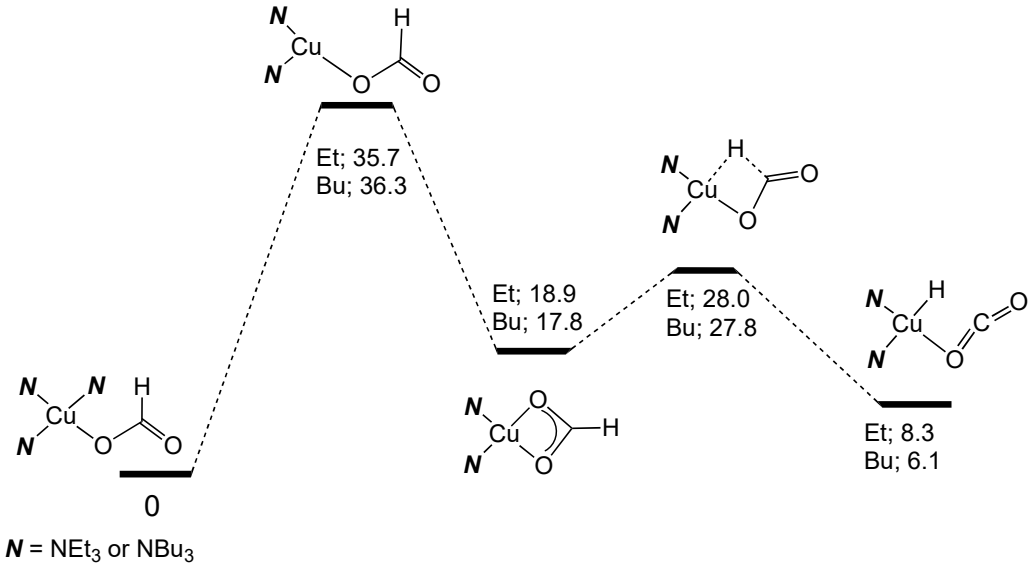

Scheme 14. Energy profile for the beta β-hydrogen elimination process to give a *cis*-[CuH$(NR_3)_2(\kappa^1$-*O*-$CO_2)$] intermediate.

The substitution of CO_2 by one molecule of NR_3 from *cis*-[CuH$(NR_3)_2(\kappa^1$-*O*-$CO_2)$] gives intermediate *cis*-[CuH$(NR_3)_3$], which reacts with FA to afford the dihydrogen-formate species *cis*-[Cu$(H_2)(NR_3)_2(\kappa^1$-*O*-$HCO_2)$]. The substitution of dihydrogen by one molecule of amine closes the catalytic cycle (Scheme 15) [44].

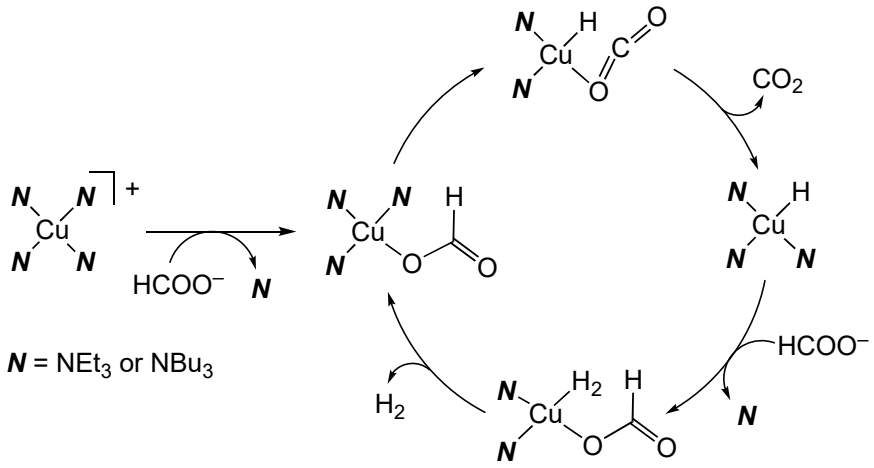

Scheme 15. Proposed catalytic cycle for the Cu(I) / NR_3 catalyzed FA dehydrogenation.

Recently, the potential of species $[CuH(phen^*)]^{2-}$ (phen* = 4,7-diphenyl-1,10-phenanth roline-disul-fonic acid disodium salt) as a catalyst for the selective decarboxylation of FA has been experimentally and theoretically studied. The sulfonate sites, which can be used as linkers for the heterogenization of these species, are far from the {CuH} reactive site and therefore should not interfere with its reactivity [45].

On the other hand, Cu(I)-dinuclear species with tetradentate phosphine ligands have also been proposed as catalysts for the dehydrogenation of FA. The activity of these catalysts is moderate, with TOF values in the range of 120–700 h^{-1}. Mechanistic studies for these reactions suggested that asymmetric dinuclear species are formed during the catalytic process. Based on this outcomes, the authors proposed a reaction mechanism where the formate bridge changes from a $Cu_2(\mu$-κ-*O*,*O*′-$O_2CH)$ to a $Cu_2(\mu$-κ-*O*-$O_2CH)$ coordination mode (Scheme 16) [46].

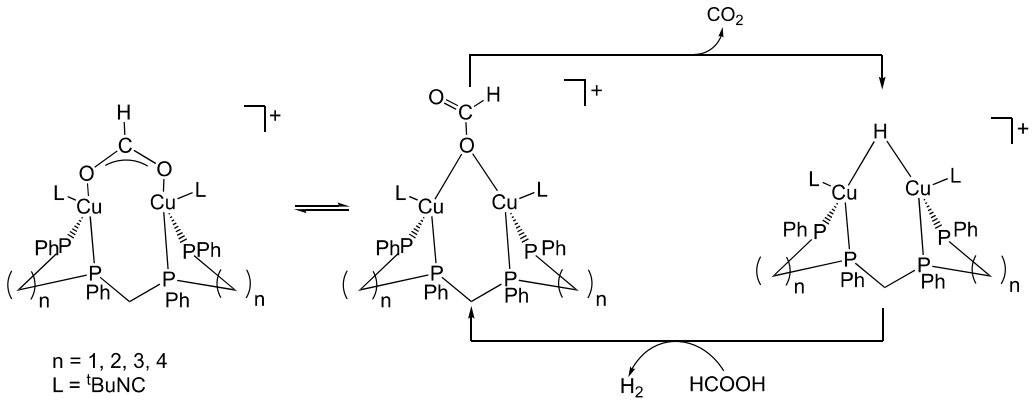

Scheme 16. Proposed catalytic cycle for Cu_2-(P_4) catalyzed dehydrogenation of FA.

3. Miscellaneous

3.1. Aluminum and Boron Homogeneous Catalysts

It is noteworthy that catalysts for the dehydrogenation of FA based on main-group elements have also been reported. Al-complex **33**, which features an NNN participative ligand, proved active in a variety of solvents using Et_3N as an additive [47]. The best activities were observed in tetrahydrofurane at 65 °C using a 0.006 mol% of **33** and a HCOOH:Et_3N mixture (5:2), which bring about a TOF of 5200 h^{-1} and a TON_{1h} of 2200. Detailed mechanistic investigation led the authors to propose the catalytic cycle depicted in Scheme 10. The pre-catalyst **33** reacts with FA to afford the resting state, **34**, which presents a neutral NNN ligand formed by double protonation of the dianionic ligand in the parent complex. β-hydride elimination generates CO_2 and an Al-hydride intermediate (**35**). For this step, the authors postulate a transition state where the formate ligand dissociates to interact by hydrogen bond with the N-H moiety of the NNN ligand, thus allowing hydride abstraction by the Al-center (**TS34-35**). Finally, protonation of the hydride ligand by FA yields H_2 and regenerates the resting state (Scheme 17).

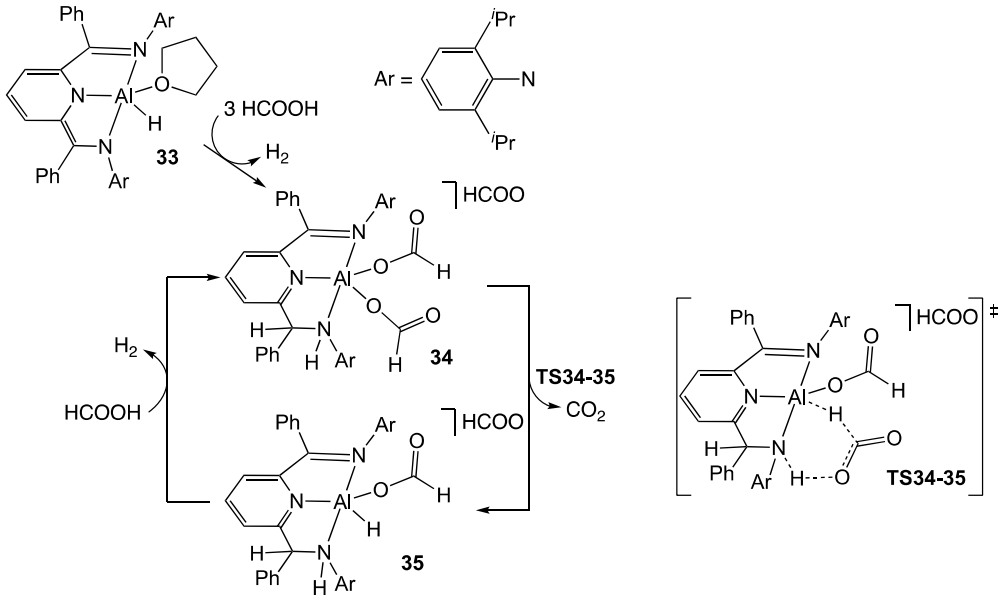

Scheme 17. Catalytic cycle proposed for the dehydrogenation of FA using **33** as catalyst. The symbol "‡" denotes a transition state.

Although boron is not a metal and the activities so far reported by catalysts based on this semimetal are modest, we believe that it is interesting to highlight the progress

realized in this area because of the great promise for future development. Recent work by Cantat and coworkers describes the activity of dialkylborane derivatives in the presence of a HCOOH:Et_3N mixture (5:2) in various solvents at 130 °C. The best activity was obtained for $[Cy_2B(OOCH)_2][Et_3NH]$ (**35**) in acetonitrile, allowing a TON of 100 after 26 h [48]. The authors proposed a catalytic cycle based on DFT studies that entails the formation of **I21** by dissociation of formate, which allows the decarboxylation step to take place by hydride abstraction to give an active Cy_2BH intermediate that reacts with one formate ion to generate **I22**, which undergoes protonation of the hydride by FA to yield H_2 and **I21** (Scheme 18).

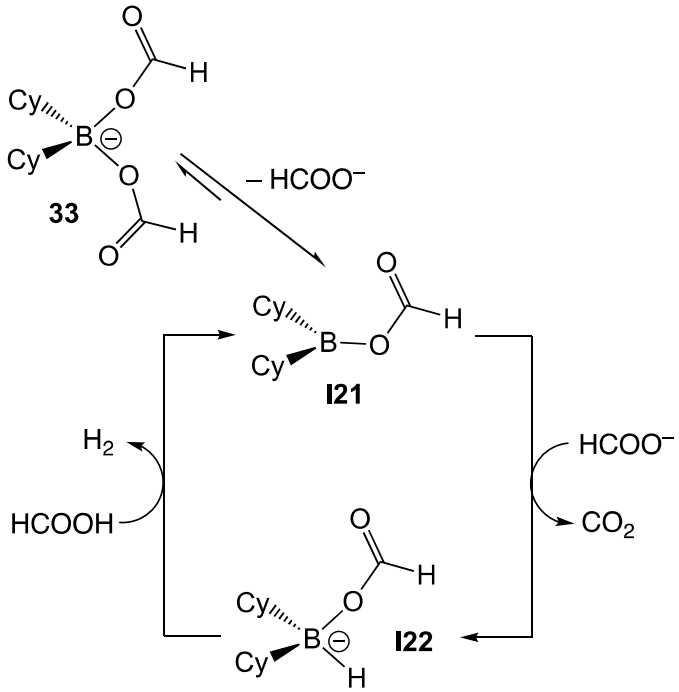

Scheme 18. Catalytic cycle proposed for the dehydrogenation of FA using **32** as catalyst.

3.2. Heterodinuclear Homogeneous Catalysts

Heterodinuclear complexes featuring an Ir(III) center with a Co (**36**), Ni (**37**) or Cu (**38**) atom in the vicinity show a dramatic increase of their activity compared to the related mononuclear Ir(III) complex **39** (Figure 5) [49]. The highest synergistic effect was observed for Ni, with **36**, **37** and **38** showing TOF values of 57, 72 and 26 h^{-1}, respectively. These TOF values sharply contrast with that of the mononuclear Ir(III) complex **39** (0.26 h^{-1}).

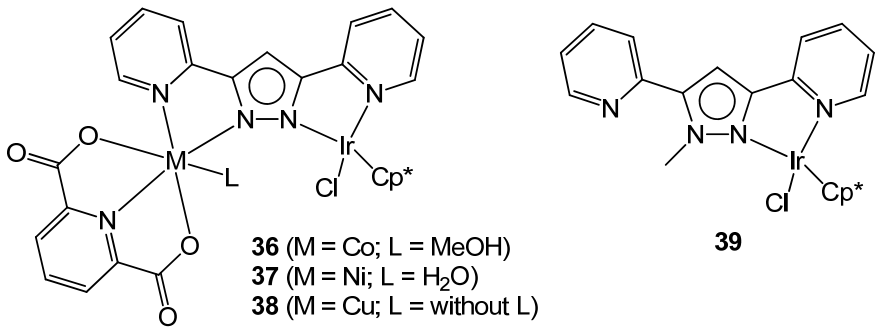

Figure 5. Depiction of complexes **36–39**.

The authors proposed a reaction mechanism for **37** that entails the formation of a cationic aquocomplex (**I23**) that reversively coordinates a formate to give (**I24**). Subse-

quently, β-hydride elimination affords **I25** upon coordination of a molecule of water. Finally, protonation of the hydride ligand at the Ir center by H_3O^+, which is the rate limiting step, closes the catalytic cycle (Scheme 19).

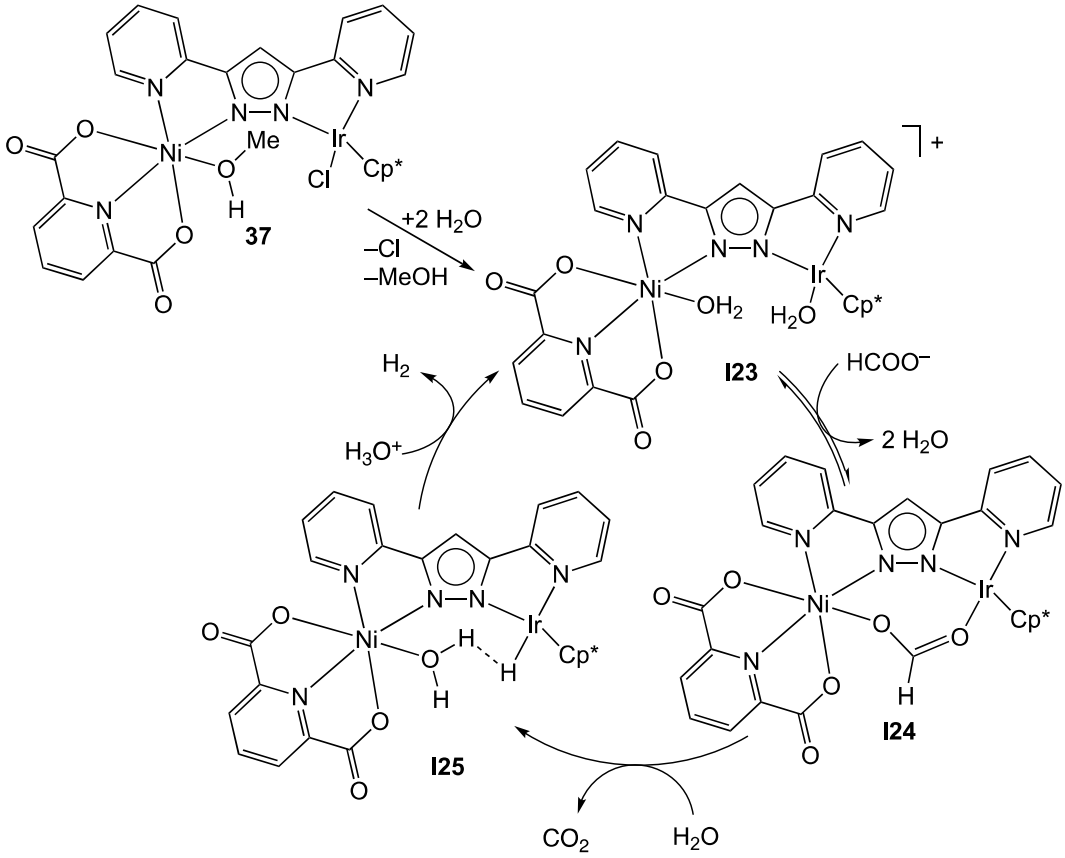

Scheme 19. Catalytic cycle proposed for the dehydrogenation of FA using **37** as catalyst.

4. Conclusions

In recent years, several examples of outstanding catalytic systems for FADH based on EAM have been developed. The most active EAM-catalysts are those that use iron as the metal center, followed by manganese and cobalt.

Regarding the mechanisms that operate in these reactions, although participative ligands do play an important role in many cases, they are not imperative to design active catalysts. In this regard, the decarboxylation step in FADH—which usually takes place by hydride abstraction or β-elimination—is often described as the rate determining step, not only for EAM, but also for PGM. Therefore, the use of bifunctional catalysts or additives that facilitate this step may boost the catalytic activity of the system. Hydride abstraction has been described to be favored by outer-sphere interactions that stabilize a transition state whose formation requires a formate ligand to flip over, changing from a stable *O*-coordination mode to an unfavorable M-H interaction. This review shows examples of this stabilization taking place by hydrogen bond between the formate and an N-H fragment of a participative ligand, or by interaction of the formate with Lewis acid additives. In both cases, the negative charge at the carboxylate moiety is stabilized, thus facilitating an M-H interaction that enables the hydride abstraction step. The H_2 formation step may be assisted by ligands able to establish a hydrogen bond interaction with the carbonyl moiety of FA, which places the acidic OH proton in the proximity of the hydride, thus enabling hydride protonation by a low energy pathway. Protonation of the hydride ligand has also been proposed to be favored by the presence of water, since the hydronium ion protonates the hydride more straightforwardly than FA.

In conclusion, there is still much room for improvement in this field regarding the activity and stability of EAM-catalysts. Moreover, although some Fe systems show excellent activities, none of the examples so far reported can operate in neat FA, which is crucial for practical applications, since the use of a solvent reduces the hydrogen density of the mixture. The examination of the catalytic systems reviewed here suggests that ligand design is fundamental to improving the catalyst performance by stabilizing the active species or by assisting key steps via outer-sphere interactions. Therefore, regarding future challenges and opportunities, EAM complexes that present ligands capable of assisting key steps of the catalytic cycle by non-covalent interactions are firm candidates for achieving enhanced activities—the final goal being the preparation of robust catalysts able to accomplish activities in neat FA comparable to those obtained by their PGM counterparts.

Author Contributions: Conceptualization, M.I. and F.J.F.-A.; methodology, M.I. and F.J.F.-A.; software, M.I. and F.J.F.-A.; validation, M.I. and F.J.F.-A.; formal analysis, M.I. and F.J.F.-A.; investigation, M.I. and F.J.F.-A.; resources, M.I. and F.J.F.-A.; data curation, M.I. and F.J.F.-A.; writing—original draft preparation, M.I. and F.J.F.-A.; writing—review and editing, M.I. and F.J.F.-A.; visualization, M.I. and F.J.F.-A.; supervision, M.I. and F.J.F.-A.; project administration, M.I. and F.J.F.-A.; funding acquisition, M.I. and F.J.F.-A. All authors have read and agreed to the published version of the manuscript.

Funding: The financial support from projects RTI2018-099136-A-I00 and PGC2018-099383-B-I00 (MCIU/AEI/FEDER), as well as Gobierno de Aragón project E42_20R, is gratefully acknowledged.

Institutional Review Board Statement: Not applicable.

Informed Consent Statement: Not applicable.

Data Availability Statement: Not applicable.

Conflicts of Interest: The authors declare no conflict of interest.

References

1. Bullock, R.M.; Chen, J.G.; Gagliardi, L.; Chirik, P.J.; Farha, O.K.; Hendon, C.H.; Jones, C.W.; Keith, J.A.; Klosin, J.; Minteer, S.D.; et al. Using nature's blueprint to expand catalysis with Earth-abundant metals. *Science* **2020**, *369*, eabc3183. [CrossRef] [PubMed]
2. Albrecht, M.; Bedford, R.; Plietker, B. Catalytic and Organometallic Chemistry of Earth-Abundant Metals. *Organometallics* **2014**, *33*, 5619–5621. [CrossRef]
3. Su, B.; Cao, Z.-C.; Shi, Z.-J. Exploration of Earth-Abundant Transition Metals (Fe, Co, and Ni) as Catalysts in Unreactive Chemical Bond Activations. *Acc. Chem. Res.* **2015**, *48*, 886–896. [CrossRef]
4. Thoi, V.S.; Sun, Y.; Long, J.R.; Chang, C.J. Complexes of earth-abundant metals for catalytic electrochemical hydrogen generation under aqueous conditions. *Chem. Soc. Rev.* **2013**, *42*, 2388–2400. [CrossRef] [PubMed]
5. Reed-Berendt, B.G.; Polidano, K.; Morrill, L.C. Recent advances in homogeneous borrowing hydrogen catalysis using earth-abundant first row transition metals. *Org. Biomol. Chem.* **2019**, *17*, 1595–1607. [CrossRef]
6. Gandeepan, P.; Cheng, C.-H. Cobalt Catalysis Involving π Components in Organic Synthesis. *Acc. Chem. Res.* **2015**, *48*, 1194–1206. [CrossRef] [PubMed]
7. Chirik, P.; Morris, R. Getting Down to Earth: The Renaissance of Catalysis with Abundant Metals. *Acc. Chem. Res.* **2015**, *48*, 2495. [CrossRef]
8. Eppinger, J.; Huang, K.-W. Formic Acid as a Hydrogen Energy Carrier. *ACS Energy Lett.* **2017**, *2*, 188–195. [CrossRef]
9. Luque-Gómez, A.; García-Abellán, S.; Munarriz, J.; Polo, V.; Passarelli, V.; Iglesias, M. Impact of Green Cosolvents on the Catalytic Dehydrogenation of Formic Acid: The Case of Iridium Catalysts Bearing NHC-phosphane Ligands. *Inorg. Chem.* **2021**, *60*, 15497–15508. [CrossRef]
10. Haider, R.; Wen, Y.; Ma, Z.-F.; Wilkinson, D.P.; Zhang, L.; Yuan, X.; Song, S.; Zhang, J. High temperature proton exchange membrane fuel cells: Progress in advanced materials and key technologies. *Chem. Soc. Rev.* **2021**, *50*, 1138–1187. [CrossRef]
11. Baschuk, J.J.; Li, X. Carbon monoxide poisoning of proton exchange membrane fuel cells. *Int. J. Energy Res.* **2001**, *25*, 695–713. [CrossRef]
12. Iglesias, M.; Oro, L.A. Mechanistic Considerations on Homogeneously Catalyzed Formic Acid Dehydrogenation. *Eur. J. Inorg. Chem.* **2018**, 2125–2138. [CrossRef]
13. Li, J.; Li, J.; Zhang, D.; Liu, C. DFT Study on the Mechanism of Formic Acid Decomposition by a Well-Defined Bifunctional Cyclometalated Iridium(III) Catalyst: Self-Assisted Concerted Dehydrogenation via Long-Range Intermolecular Hydrogen Migration. *ACS Catal.* **2016**, *6*, 4746–4754. [CrossRef]

14. Cohen, S.; Borin, V.; Schapiro, I.; Musa, S.; De-Botton, S.; Belkova, N.V.; Gelman, D. Ir(III)-PC(sp^3)P Bifunctional Catalysts for Production of H_2 by Dehydrogenation of Formic Acid: Experimental and Theoretical Study. *ACS Catal.* **2017**, *7*, 8139–8146. [CrossRef]
15. Iturmendi, A.; Rubio-Pérez, L.; Pérez-Torrente, J.J.; Iglesias, M.; Oro, L.A. Impact of Protic Ligands in the Ir-Catalyzed Dehydrogenation of Formic Acid in Water. *Organometallics* **2018**, *37*, 3611–3618. [CrossRef]
16. Matsunami, A.; Kuwata, S.; Kayaki, Y. A Bifunctional Iridium Catalyst Modified for Persistent Hydrogen Generation from Formic Acid: Understanding Deactivation via Cyclometalation of a 1,2-Diphenylethylenediamine Motif. *ACS Catal.* **2017**, *7*, 4479–4484. [CrossRef]
17. Wang, W.-H.; Xu, S.; Manaka, Y.; Suna, Y.; Kambayashi, H.; Muckerman, J.T.; Fujita, E.; Himeda, Y. Formic Acid Dehydrogenation with Bioinspired Iridium Complexes: A Kinetic Isotope Effect Study and Mechanistic Insight. *ChemSusChem* **2014**, *7*, 1976–1983. [CrossRef] [PubMed]
18. Oldenhof, S.; Lutz, M.; de Bruin, B.; van der Vlugt, J.I.; Reek, J.N.H. Dehydrogenation of formic acid by Ir–bisMETAMORPhos complexes: Experimental and computational insight into the role of a cooperative ligand. *Chem. Sci.* **2015**, *6*, 1027–1034. [CrossRef]
19. Sordakis, K.; Tang, C.; Vogt, L.K.; Junge, H.; Dyson, P.J.; Beller, M.; Laurenczy, G. Homogeneous Catalysis for Sustainable Hydrogen Storage in Formic Acid and Alcohols. *Chem. Rev.* **2018**, *118*, 372–433. [CrossRef] [PubMed]
20. Laurenczy, G.; Dyson, P.J. Homogeneous Catalytic Dehydrogenation of Formic Acid: Progress Towards a Hydrogen-Based Economy. *J. Braz. Chem. Soc.* **2014**, *25*, 2157–2163. [CrossRef]
21. Guan, C.; Pan, Y.; Zhang, T.; Ajitha, M.J.; Huang, K.-W. An Update on Formic Acid Dehydrogenation by Homogeneous Catalysis. *Chem. Asian J.* **2020**, *15*, 937–946. [CrossRef] [PubMed]
22. Grasemann, M.; Laurenczy, G. Formic acid as a hydrogen source—Recent developments and future trends. *Energy Environ. Sci.* **2012**, *5*, 8171–8181. [CrossRef]
23. Stathi, P.; Solakidou, M.; Louloudi, M.; Deligiannakis, Y. From Homogeneous to Heterogenized Molecular Catalysts for H_2 Production by Formic Acid Dehydrogenation: Mechanistic Aspects, Role of Additives, and Co-Catalysts. *Energies* **2020**, *13*, 733. [CrossRef]
24. Tamarany, R.; Shin, D.Y.; Kang, S.; Jeong, H.; Kim, J.; Kim, J.; Yoon, C.W.; Lim, D.-H. Formic acid dehydrogenation over PdNi alloys supported on N-doped carbon: Synergistic effect of Pd–Ni alloying on hydrogen release. *Phys. Chem. Chem. Phys.* **2021**, *23*, 11515–11527. [CrossRef] [PubMed]
25. Liab, J.; Zhua, Q.-L.; Xu; Q. Dehydrogenation of Formic Acid by Heterogeneous Catalysts. *Chimia* **2015**, *69*, 348–352. [CrossRef]
26. Onishi, M. Decomposition of formic acid catalyzed by hydrido (phosphonite) cobalt (I) under photoirradiation. *J. Molec. Catal.* **1993**, *80*, 145–149. [CrossRef]
27. Zhou, W.; Wei, Z.; Spannenberg, A.; Jiao, H.; Junge, K.; Junge, H.; Beller, M. Cobalt-Catalyzed Aqueous Dehydrogenation of Formic Acid. *Chem. Eur. J.* **2019**, *25*, 8459–8464. [CrossRef] [PubMed]
28. Junge, K.; Wendt, B.; Cingolani, A.; Spannenberg, A.; Wei, Z.; Jiao, H.; Beller, M. Cobalt Pincer Complexes for Catalytic Reduction of Carboxylic Acid Esters. *Chem. Eur. J.* **2018**, *24*, 1046–1052. [CrossRef]
29. Lentz, N.; Aloisi, A.; Thuéry, P.; Nicolas, E.; Cantat, T. Additive-Free Formic Acid Dehydrogenation Catalyzed by a Cobalt Complex. *Organometallics* **2021**, *40*, 565–569. [CrossRef]
30. Cook, A.W.; Emge, T.J.; Waldie, K.M. Insights into Formate Oxidation by a Series of Cobalt Piano-Stool Complexes Supported by Bis(phosphino)amine Ligands. *Inorg. Chem.* **2021**, *60*, 7372–7380. [CrossRef]
31. Boddien, A.; Loges, B.; Gärtner, F.; Torborg, C.; Fumino, K.; Junge, H.; Ludwig, R.; Beller, M. Iron-Catalyzed Hydrogen Production from Formic Acid. *J. Am. Chem. Soc.* **2010**, *132*, 8924–8934. [CrossRef]
32. Boddien, A.; Mellmann, D.; Gärtner, F.; Jackstell, R.; Junge, H.; Dyson, P.J.; Laurenczy, G.; Ludwig, R.; Beller, M. Efficient dehydrogenation of formic acid using an iron catalyst. *Science* **2011**, *333*, 1733–1736. [CrossRef] [PubMed]
33. Bielinski, E.A.; Lagaditis, P.O.; Zhang, Y.; Mercado, B.Q.; Würtele, C.; Bernskoetter, W.H.; Hazari, N.; Schneider, S. Lewis Acid-Assisted Formic Acid Dehydrogenation Using a Pincer-Supported Iron Catalyst. *J. Am. Chem. Soc.* **2014**, *136*, 10234–10237. [CrossRef]
34. Curley, J.B.; Smith, N.E.; Bernskoetter, W.H.; Hazari, N.; Mercado, B.Q. Catalytic Formic Acid Dehydrogenation and CO_2 Hydrogenation Using Iron PN^RP Pincer Complexes with Isonitrile Ligands. *Organometallics* **2018**, *37*, 3846–3853. [CrossRef]
35. Bertini, F.; Mellone, I.; Ienco, A.; Peruzzini, M.; Gonsalvi, L. Iron(II) Complexes of the Linear *rac*-Tetraphos-1 Ligand as Efficient Homogeneous Catalysts for Sodium Bicarbonate Hydrogenation and Formic Acid Dehydrogenation. *ACS Catal.* **2015**, *5*, 1254–1265. [CrossRef]
36. Tondreu, A.M.; Boncella, J.M. 1,2-Addition of Formic or Oxalic Acid to $-N\{CH_2CH_2(PiPr_2)\}_2$-Supported Mn(I) Dicarbonyl Complexes and the Manganese-Mediated Decomposition of Formic Acid. *Organometallics* **2016**, *35*, 2049–2052. [CrossRef]
37. Anderson, N.H.; Boncella, J.; Tondreau, A.M. Manganese-Mediated Formic Acid Dehydrogenation. *Chem. Eur. J.* **2019**, *25*, 10557–10560. [CrossRef] [PubMed]
38. Lèval, A.; Agapova, A.; Steinlechner, C.; Alberico, E.; Junge, H.; Beller, M. Hydrogen production from formic acid catalyzed by a phosphine free manganese complex: Investigation and mechanistic insights. *Green Chem.* **2020**, *22*, 913–920. [CrossRef]
39. Lèval, A.; Junge, H.; Beller, M. Manganese(i) κ_2-NN complex-catalyzed formic acid dehydrogenation. *Catal. Sci. Technol.* **2020**, *10*, 3931–3937. [CrossRef]

40. Britto, N.J.; Jaccob, M. Deciphering the Mechanistic Details of Manganese-Catalyzed Formic Acid Dehydrogenation: Insights from DFT Calculations. *Inorg. Chem.* **2021**, *60*, 11038–11047. [CrossRef]
41. Enthaler, S.; Brück, A.; Kammer, A.; Junge, H.; Irran, E.; Gülak, S. Exploring the Reactivity of Nickel Pincer Complexes in the Decomposition of Formic Acid to CO_2/H_2 and the Hydrogenation of $NaHCO_3$ to NaOOCH. *ChemCatChem* **2015**, *7*, 65–69. [CrossRef]
42. Neary, M.C.; Parkin, G. Nickel-catalyzed release of H_2 from formic acid and a new method for the synthesis of zerovalent $Ni(PMe_3)_4$. *Dalton Trans.* **2016**, *45*, 14645–14650. [CrossRef] [PubMed]
43. Scotti, N.; Psaro, R.; Ravasio, N.; Zaccheria, F. A new Cu-based system for formic acid dehydrogenation. *RSC Adv.* **2014**, *4*, 61514–61517. [CrossRef]
44. Correa, A.; Cascella, M.; Scotti, N.; Zacheria, F.; Ravasio, N.; Psaro, R. Mechanistic insights into formic acid dehydrogenation promoted by Cu-amino based systems. *Inorg. Chim. Acta.* **2018**, *470*, 290–294. [CrossRef]
45. O'Hair, R.A.J.; Mravak, A.; Krstić, M.; Bonačić-Koutecký, V. Models Facilitating the Design of a New Metal-Organic Framework Catalyst for the Selective Decomposition of Formic Acid into Hydrogen and Carbon Dioxide. *ChemCatChem* **2019**, *11*, 2443–2448. [CrossRef]
46. Nakajima, T.; Kamiryo, Y.; Kishimoto, M.; Nakamae, K.; Ura, Y.; Tanase, T. Synergistic Cu_2 Catalysts for Formic Acid Dehydrogenation. *J. Am. Chem. Soc.* **2019**, *141*, 8732–8736. [CrossRef]
47. Myers, T.W.; Berben, L.A. Aluminium–ligand cooperation promotes selective dehydrogenation of formic acid to H_2 and CO_2. *Chem. Sci.* **2014**, *5*, 2771–2777. [CrossRef]
48. Chauvier, C.; Tlili, A.; Das Neves Gomes, C.; Thuéry, P.; Cantat, T. Metal-free dehydrogenation of formic acid to H_2 and CO_2 using boron-based catalysts. *Chem. Sci.* **2015**, *6*, 2938–2942. [CrossRef] [PubMed]
49. Hong, D.; Shimoyama, Y.; Ohgomori, Y.; Kanega, R.; Kotani, H.; Ishizuka, Y.; Kon, Y.; Himeda, Y.; Kojima, T. Cooperative Effects of Heterodinuclear IrIII−MII Complexes on Catalytic H_2 Evolution from Formic Acid Dehydrogenation in Water. *Inorg. Chem.* **2020**, *59*, 11976–11985. [CrossRef]